



Norwegian University of
Science and Technology

Model based estimation of the complex material constants for thickness extension and radial mode in an ultrasound disk transducer

Eivind Solbakken Tjelde

Master of Science in Electronics

Submission date: Januar 2012

Supervisor: Trond Ytterdal, IET

Co-supervisor: Tonni Franke Johansen, ISB

Problem Description

The student shall investigate model based estimation of material parameters of ultrasound transducer. Material parameters shall be estimated based on measurement of electrical impedance of a piezoelectric disc or a layered material with at least one piezoelectric disc. The models of the transducers shall be either analytical expressions or based on a 1D Mason based model (xTrans).

The target is to achieve robust estimates of the following material parameters:

- Piezoelectric material
 - complex thickness mode constants: piezoelectric constant, dielectric constant and elasticity constant.
 - complex transverse mode constants, piezoelectric constant, dielectric constant and elasticity constant
- Elastic layers, that is bonding, matching layers, and backing
 - complex thickness mode constants: mechanical elasticity constant.

Uncertainty measures for the measurements shall be investigated. The student shall develop a MATLAB program for interactive control of the characterization.

Trondheim, August 2011

Preface

This thesis is part of my master degree at Department of Electronics and Telecommunication at the Norwegian University of Science and Technology (NTNU). I would like to thank my supervisor Tonni Franke Johansen for his patience, and his guidance in the fields of acoustics and piezoelectrics, and Ketil Joner for his lab experience during sample preparation. Sigvald Marholm should also be mentioned for our great discussions in the field of mathematics and Matlab.

Trondheim, January 2012
Eivind Solbakken Tjelde

Abstract

The main goal of this thesis is to establish a method and estimate the complex material constants for the radial and thickness mode. This has been done in two separate methods. For the thickness mode material constants, a optimization script in MATLAB has been developed, which is capable of directly optimizing all the input parameters for the xTrans, for both active and passive layers. The method has been evaluated, and the complex material constants describe behavior in accordance with measured data. For estimating the radial mode complex material constants, an evaluation a publish method by S.Sheritt has been done.

Contents

1	Introduction	1
1.1	Scope	1
1.2	Purpose	2
2	Theory	4
2.1	Basic concepts of a piezoelectric transducer	4
2.1.1	Structural description	4
2.1.2	Mode of operation	5
2.1.3	Establishing name system	6
2.2	Piezoelectric theory	8
2.2.1	Piezoelectric material	8
2.2.2	Mode of operation	9
2.3	Real and imaginary material constants of piezoelectric resonators	11
2.3.1	Loss	12
2.4	Optimization	13
2.4.1	Introduction Optimization	13
2.4.2	Nelder-Mead Algorithm and FMINSEARCH	13
2.5	Uncertainty measurements	14
3	Estimation methods and equipment	15
3.1	Impedance Measurements	15
3.2	Fabrication process at ISB	15
3.3	xTrans	16
3.4	Simulation method for finding the complex thickness parameters	16
3.4.1	Implementation of the software	16
3.4.2	Simulation procedure	17
3.5	Method derived by Sherrit for deriving the radial complex parameters	20
4	Results	21
4.1	Estimates of the complex material constants for thickness mode	21
4.1.1	Graphical representation of the admittance	21
4.1.2	Sources of error	21
4.1.3	Comparison of the modeled admittance curve and the measured	24
4.1.4	SEM inspection of the samples	24
4.1.5	Derived material constants	26
4.2	Evaluation of the complex material constants in the radial mode	27

5 Discussion	30
6 Conclusion and Further Work	32
A Accuracy on the calculation script	35
B SEM inspection of a transducer sample	36

List of Figures

2.1	Structural overview of a piezoelectric transducer [2]	5
2.2	Structural overview of a transducer and all its layers.	7
2.3	Overview of the perovskite crystal structure in PZT [22]	8
2.4	Simplified tensor notation used in this report	9
2.5	Determination of the critical frequencies by admittance and impedance plot [14]	11
3.1	Simulation flow	17
3.2	Illustrating some of the challenges. <code>lm3VSlm4</code>	19
4.1	Sample 4 Simulated for PZT layer	23
4.2	Sample 4 Simulated for ML1 layer	24
4.3	Sample 4 Simulated for ML2 layer	25
4.4	Comparison of the complex material constants and the real to the measured data	25
4.5	Same as above but zooming in on the essential parts	26
4.6	loglog plot of sample 4, which shows great fit	28
4.7	Sample 4	29
B.1	The edge	36
B.2	Showing the consisting of glue and air	37
B.3	SEM3	38
B.4	SEM4	39
B.5	SEM5	40
B.6	SEM6	41
B.7	PZT grain size	42

List of Tables

2.1	Description of the name structure	7
2.2	The relation between the piezoelectric constants.[2]	11
3.1	The input value for the start up procedure	19
4.1	Comparison of the real simulated parameters vs. datasheet	22
4.2	The tolerances from the manufacturer	22
4.3	A statistical representation of the material constants for the piezoelectric disk	22
4.4	A statistical representation of the material constants for the Matching Layer 1	22
4.5	A statistical representation of the material constants for the Matching Layer 2	23
4.6	A statistical representation of the thickness of the glue	23
4.7	Comparison of c33d	27
4.8	The result from samples used.	27
4.9	Uncertainty calculations of the calculated parameters	28
A.1	Comparison of the parametsr given in the paper and the one calculated with the developed radial script	35

List of Symbols

<i>Name</i>	<i>Type</i>	<i>unit</i>
p	pressure	
S	strain	
D	electric displacement	
E	electric field	
T	tension	
d,e,g,h	piezoelectric constants	
c	mechanical stiffness constant	
s	mechanical compliance constant	
ε	dielectric constant	
k_t	electromechanical coupling factor for thickness mode	
t	time	
λ	wavelength	
f	frequency	
f_p	parallel frequency	
f_s	serial frequency	
n	harmonic order	
L	length	
A	areal	
$Z(\omega)$	impedance as a function of angular frequency	
$\varepsilon_0 = 8.854 * 10^{-12}$ (F/m)	permittivity of free space	

A superscript notation indicates that this variable is constant in the measurement. For tensor notation see 2.2.2

Chapter 1

Introduction

A piezoelectric ultrasonic transducer employs a piezoelectric material to convert electrical energy into mechanical energy and vice versa. The properties of the piezoelectric material have great impact on the behavior of the transducer, making the understanding of said properties essential in the analysis and design of transducers. It is of utmost importance to develop high quality transducers, as the signal processing is ultimately limited by the quality of the input signal.

1.1 Scope

In medical ultrasound imaging, sound waves with frequencies above the audible range of human hearing are utilized to visualize subcutaneous body structures. The use of obstetric sonography during pregnancy is widely recognized by the public, however ultrasound is also serving as a visualizing tool in many medical fields among others during endoscopic surgery and echocardiography.

The recent development in the field of medical technology has resulted in instruments which makes it possible to examine the inside of the blood vessels[12], and the construction of a miniaturized robotic pill for advanced diagnostics and therapy within the human digestive tract, making a significant contribution to the diagnosis and treatment of digestive cancers [20]. Another recent innovative product is the pocket-sized Vscan by GE Vingmed Ultrasound, which is capable of visualizing blood flow in addition to monochromatic anatomic images in real time. In addition to create innovative products, the development in this field also concerns making consisting products smaller, with better portability and lower costs[13]. This leads to a constant demand for a improved transducer technology, with new features and better specifications.

The transducer is a device that converts one energy domain to another. Related to medical ultrasound, the transducer operates as both microphone and a loudspeaker, converting sound waves from incoming fluctuations in air pressure to an electrical signal and vice versa. The property that makes this possible for a piezoelectric transducer, is the ability of the material to translate the exposure of mechanical stress into generation of electrical charges. That enables us to represent the invisible sound echoes received by the transducer into graphical

pictures and animations, that are much easier for humans to extract information from and interpret.

The innovation in the field of ultrasound transducers is aided by new production methods and state of the art technology from other fields such as nanotechnology. This has given rise to a more controlled production process, but the complexity has increased as well. As a consequence there are even more process parameters that can be tuned, and better knowledge in this process optimization will result in better transducers.

Many practical and theoretical problems will usually occur in the process of designing new technology. At Department of circulation and medical imaging the designed transducers were previously produced externally, which did not allow full access to all process data, and resulted in a lack of information about the construction process. In order to deal with this problem, and be able to get more information out of the process, the department decided to make their own lab. This has resulted in a transducer lab with dedicated personnel, which is partly funded by GE Vingmed, with the motivation to get more insight into the production process to be able to tune the process parameters as required.

1.2 Purpose

The behavior of an ultrasound transducer is complex and dependent on many parameters such as electrical, mechanical and other material properties. Through the use of mathematical modeling the behavior can be simulated and then better understood. At Department of circulation and medical imaging there has been developed a special MATLAB program aimed for transducer modeling, named xTrans. This is a 1D Mason based model, that aloud a user to simulate the behavior of a designed transducer, given the structure and its material constants as input.

In order to get a proper model of the transducer the input parameters have to be carefully selected from measurements on a representative sample. Not every part of the transducer can be measured, for instance the thickness of the glue layer that attach the structure together, and the amount of air that fills the cavity due to surface roughness. Although the final behavior is dependent on these effects, and a proper model has to take such effects into consideration. To meet this challenge, these non measurable parameters has to be estimated.

The main focus in this thesis is to investigate model based estimation of material parameters, based on measurements on the electrical impedance. In the production process, before a new layered structure was attached, measurements of the electrical impedance was taken. These data give insight in the changing condition of the impedance during production, and enables us to extract information about the different structure in the transducer.

The estimation will be performed by letting an optimization algorithm minimize the error between the measured data and the transducer model outcome, by choosing the best fitting material parameters. The goal is to achieve complex material parameters, that have the advantage to contain information about its loss properties. This is an essential property of the parameters, and by generating complex parameters the loss will be addressed to each parameter in particular instead of having one general loss factor. These complex parameters are yet to be unacquainted, since the manufacturer only publishes real material constants.

Therefore, part of the work in this thesis will be to design a suitable optimization script that communicates with the xTrans model and iterates through possible material constants combinations.

This thesis covers the most important parameters concerning the piezoelectric layers with thickness mode resonance, including matching layers. Based on the impedance and the thickness of the transducer layers, the optimization will generate constants for the piezoelectric and dielectric constants, and the Q factor for each layer. Furthermore a procedure in how to apply the optimization script has to be set up, in order to control the optimization script.

In addition to thickness mode material constants, the parameters concerning radial mode will also be evaluated, by a method derived by S. Sherrit. By finding both radial and thickness mode material constants, we are able to clarify their interaction to each other.

Chapter 2

Theory

2.1 Basic concepts of a piezoelectric transducer

A more complete introduction to piezoelectric ultrasound transducers can be found in [2, Chapter 3], but a brief introduction is given to support the topics covered in this thesis. This section also point out the name system used in this thesis to describe the material constants for the different layers in the transducer.

2.1.1 Structural description

Figure 2.1 shows the transducer consisting of a backing layer with characteristic impedance Z_B connected to the back of the piezoelectric layer, which in turn has a characteristic impedance Z_0 . On each face of the piezoelectric layer the surface is metalized forming thin electrodes for applying voltage across the layer. In order to optimize the energy transfer between the transducer and into the load, it is common to apply matching layer/-s in between, that will reduce the impedance mismatch and also increase the bandwidth.

In order to deal with the mismatch problem, a matching layer can be inserted to improve the boundary transition. Tissue, which is often the load, has a low impedance of around $1.6M\text{Rayl}$, while the piezoelectric layer has an impedance $Z_0 \approx 33M\text{Rayl}$. The impedance can be described by Eq 2.1. This large mismatch reduces the efficient coupling of vibration energy, and makes the bandwidth of this energy coupling very narrow, which in turn will cause ringing. To increase the bandwidth (which will decrease the signal length, because $T_p \propto \frac{1}{B_w}$) a matching layer can be placed between the piezoelectric layer and the load.

$$Z = \rho c \tag{2.1}$$

$$R_{01} = \frac{Z_1 - Z_0}{Z_0 + Z_1} \tag{2.2}$$

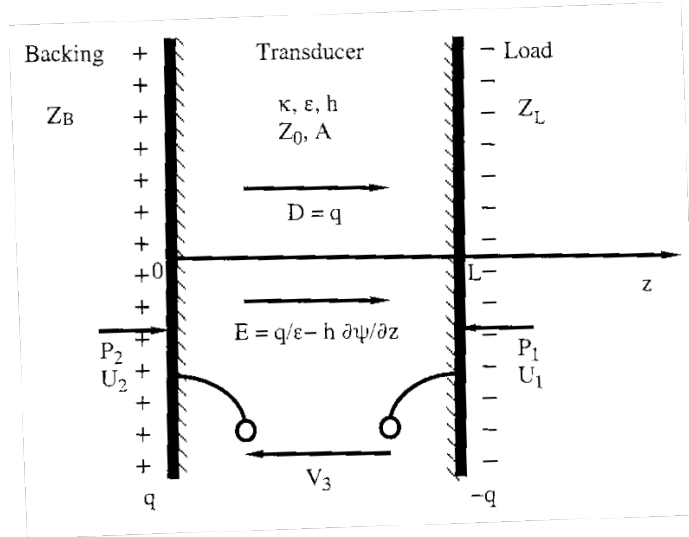


Figure 2.1: Structural overview of a piezoelectric transducer [2]

Another way to reduce the ringing problem and increase the bandwidth is by applying a backing material with higher impedance than the crystal. Although the piezoelectric layer is particularly effective at its resonance frequency, impedance mismatch between the piezoelectric layer and the load will cause some of the energy to be reflected, in accordance with Eq 2.2, and reduce the total energy transferred.

2.1.2 Mode of operation

The governing mechanism of the piezoelectric transducer is the piezoelectric effect. When voltage is applied to the electrodes on each side of the piezoelectric layer, it causes the layer to expand and contract in accordance with its polarity. The fact that the piezoelectric effect is reversible, enables the transducer to be a transmitter and a receiver at the same time. To transmit a signal, the piezoelectric layer converts an electrical AC signal into acoustic waves, and in receiving mode the transducer intercepts reflected acoustical waves and convert them into electrical signals which can be further processed and visualized.

The coupling between electrical field and strain is also affected by the way the structures are clamped. Given the structure on Figure 2.1 with electrodes connected to each face, the transducer behaves as a capacitor, see Eq 3.3, with the piezoelectric layer as the dielectric. Depending on the suspension, this will define the free capacitance or free dielectric constant, when there are no restrictions on the strain in the material, and clamped capacitance or clamped dielectric constant, obtained when the strain is zero, see Eq 2.4. For ultrasound transducers the material is commonly polarized in the direction normal to the faces that vibrate in thickness mode. This is known as transversal clamping, defined by the strain normal to the propagation being zero.

The transducer is most effective at its resonance frequency. According to [2], resonance is obtained when the combined reflection and propagation phase shifts are $2n\pi$. What really takes place in the material when resonance occur is that a bidirectional wave arise in the

piezoelectric layer and give rise to a certain pressure on the surface to achieve a higher particle velocity and thereby a more effective energy transfer between the piezoelectric layer and the load.

For a piezoelectric material the resonant frequency will also be affected by the electrical conditions, as an applied voltage across the electrodes will reduce the mechanical compression. The amount of reduction depends on the impedance of the electrical termination, and the electromechanical coupling factor k_t , see Eq 2.6. It will be reduced to its minimum when the electrodes is shorted, causing the resonance frequency to become f_{s0} , called short circuit resonance. When the charges on the electrodes are constant, the resonance frequency will become what is known as the open circuit resonance, f_0 . For materials with $k_t \approx 0.5$ the relation between the two frequencies is according to [2] $f_{s0} \approx 0.9f_0$.

The transducer will have a thickness mode resonance frequency determined by the piezoelectric layer thickness L , with the first resonance frequency occurring when the thickness is equal to a half the wavelength. Given the relation between wavelength and frequency as $\lambda = c/f$, the thickness mode resonance frequency is thus [16]

$$f_0 = \frac{nc}{2L} \quad (2.3)$$

where n is an odd number and c is the acoustic wave velocity. f_0 with $n = 1$ is known as the fundamental frequency. With respect to the thickness(L) it becomes apparent by regrouping (2.3) that resonance arise when the L is odd multiples of half of the wavelength. Similarly for the radial mode resonance frequencies which will propagate normal to the thickness mode, can also be described by the same equation as above except that L is then the diameter of the disk.

$$\varepsilon^S = \varepsilon^T(1 - k_t^2) \quad (2.4)$$

$$C = \frac{\varepsilon A}{t} \quad (2.5)$$

$$k_t^2 = \frac{h^2 \varepsilon^S}{cD} \quad (2.6)$$

2.1.3 Establishing name system

To better separate the different material constants for the different layers, a name convention system has be made. As seen on Figure 2.2, each layer has its own dedicated parameter names. Table 2.1 gives a explanation to each parameter. These names have a connection to xTrans, which aloud the user to add multiple matching layer, herby the ending -m, because in xTrans they are registered as a matching layer. The parameters given in parentheses are those the simulation program xTrans are able to modify for each layer. Therefore zm3, is the impedance of the third matching layer in xTrans(which is later will be revealed as a glue layer).

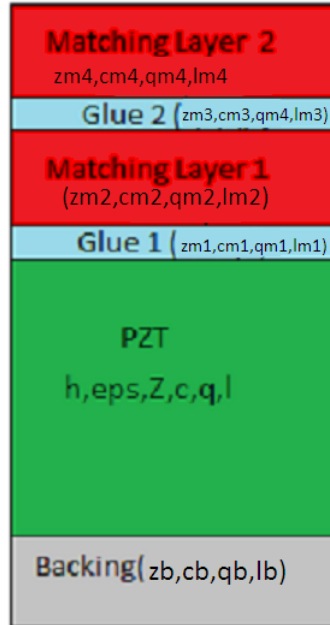


Figure 2.2: Structural overview of a transducer and all its layers.

Parameter Name	Description	Denomination
h	piezoelectric constant	10^8V/m
eps	relative dielectric constant	-
z	electrical impedance	MRayls
c	speed of sound	m/s
q	Q factor	-
l	thickness	mm

Table 2.1: Description of the name structure

2.2 Piezoelectric theory

The following section presents a brief overview of the piezoelectric effects and its behavior as a background for the model behavior. For a more complete introduction of the piezoelectric effect, see for instance [23].

2.2.1 Piezoelectric material

There are certain materials which exhibits the effect known as the piezoelectric effect. During an application of stress, these materials will generate an electrical potential difference between two conducting surfaces connected to the material. This is known as the direct piezoelectric effect[5]. The same materials will also show an inverse effect with a change in dimensions when they are subjected to an electrical field. This is known as the indirect effect. The transducer makes use of both the direct and indirect effect, when receiving and transmitting the signal respectively.

There are certain properties that have to be present in the material in order to exhibit piezoelectric effect. According to Auld[3]: “The nature of piezoelectricity is intimately connected with crystal symmetry and, in fact, cannot exist in a completely isotropic material“. The reason for this is that the piezoelectric effect is caused by displacement of microscopic charges in the crystal lattice. This motion happens in all materials, but there are only in materials with non centrosymmetric lattice structure that these displacements result in a net change of electric dipole moment per unit volume in the material, and thereby produce the piezoelectric effect. There are some effects which have certain similarities, but must not be mixed. Among them is the electrostrictive effect, causing a change in the material dimensions when exposed to an electrical field, but no change of electric charge under application of mechanical pressure, therefore no reversed effect. Another difference is that while the piezoelectric effect has a linear relation, the electrostrictive relation between electrical field and strain is nonlinear[23].

Figure 2.3 illustrates the perovskite structure of a ceramic material known as polycrystalline lead-zirconate-titanate $Pb(Zr_{1-x},Ti_x)O_3$ abbreviated PZT. This is one of the most common materials in ultrasound transducers today, and will be used in this thesis as well. For temperatures below the Curie Temperature, which is the normal working conditions for such materials, we see in the rightmost picture that the Ti^{4+} , Zr^{4+} is positioned off-center, causing a directed polarization.

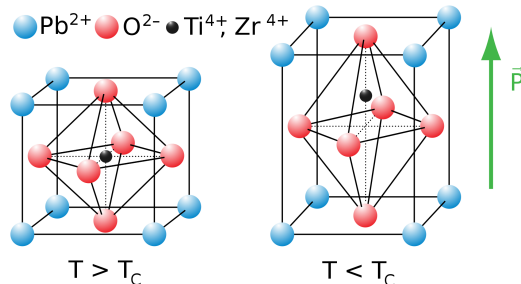


Figure 2.3: Overview of the perovskite crystal structure in PZT [22]

Some of the reasons for using PZT is its ability to generate bulk waves in MHz range[2] and its high piezoelectric coefficient d_{33} [21]. Besides from being piezoelectric, PZT also exhibits ferroelectric and pyroelectric properties.

2.2.2 Mode of operation

The behavior of the piezoelectric materials can easily be described using a combination of mechanical and electromagnetic equations.

Piezoelectric materials are anisotropic, causing their material properties to be affected by the direction in the material. As a consequence of this, the material behavior must be described by tensors, owing to the fact that there is a coupling between the different directions, linked together by material constants.

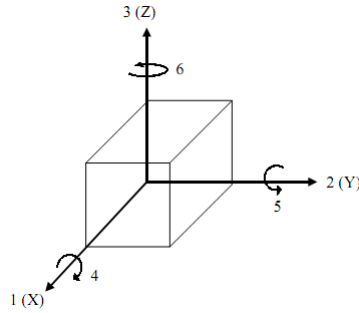


Figure 2.4: Simplified tensor notation used in this report

Mathematical description

The behavior of the piezoelectric materials can easily be described using both mechanical and electromagnetic equations. Due to the fact that a piezoelectric material is dielectric, there are no flowing charges as in conductors. This can be described by one of Maxwell's equations as Equation (2.7). The presence of an electric field in a dielectric medium will cause the polarization vectors to be reorientated, as shown by Equation (2.8)

$$\nabla \cdot \mathbf{D} = 0 \quad (2.7)$$

$$\mathbf{D} = \varepsilon_0 \mathbf{E} + \mathbf{P} \quad (2.8)$$

Considering the mechanical point of view, the relation between stress and strain follows Hooke's law as described in Equation (2.9).

$$\mathbf{T} = c_{mn} \mathbf{S} \quad (2.9)$$

Because this effect is linear, these equations can be combined, resulting in a pair of equations capable of describing the behavior of the piezoelectric material when the amplitude is small.

According to [2], the direct and indirect effect are respectively given as Equation 2.11 and Equation 2.10. A rearrangement of the initial equations will yield a total of four different but related pairs of equations. These are all listed in Equations 2.12 to 2.15. The reason for that some of the parameters is zero, is due to the fact that there are some symmetry properties in PZT. This leads to a reduction of independent variables from a total of 63 to only 10.

$$\begin{bmatrix} E_1 \\ E_2 \\ E_3 \end{bmatrix} = - \begin{bmatrix} 0 & 0 & 0 & 0 & h_{15} & 0 \\ 0 & 0 & 0 & h_{15} & 0 & 0 \\ h_{31} & h_{31} & h_{33} & 0 & 0 & 0 \end{bmatrix} \begin{bmatrix} S_1 \\ S_2 \\ S_3 \\ S_4 \\ S_5 \\ S_6 \end{bmatrix} + \begin{bmatrix} (\varepsilon_{11}^S)^{-1} & 0 & 0 \\ 0 & (\varepsilon_{11}^S)^{-1} & 0 \\ 0 & 0 & (\varepsilon_{33}^S)^{-1} \end{bmatrix} \begin{bmatrix} D_1 \\ D_2 \\ D_3 \end{bmatrix} \quad (2.10)$$

$$\begin{bmatrix} T_1 \\ T_2 \\ T_3 \\ T_4 \\ T_5 \\ T_6 \end{bmatrix} = \begin{bmatrix} c_{11}^D & c_{12}^D & c_{13}^D & 0 & 0 & 0 \\ c_{12}^D & c_{11}^D & c_{13}^D & 0 & 0 & 0 \\ c_{13}^D & c_{13}^D & c_{33}^D & 0 & 0 & 0 \\ 0 & 0 & 0 & c_{44}^D & 0 & 0 \\ 0 & 0 & 0 & 0 & c_{44}^D & 0 \\ 0 & 0 & 0 & 0 & 0 & c_{66}^D \end{bmatrix} \begin{bmatrix} S_1 \\ S_2 \\ S_3 \\ S_4 \\ S_5 \\ S_6 \end{bmatrix} - \begin{bmatrix} 0 & 0 & h_{31} \\ 0 & 0 & h_{31} \\ 0 & 0 & h_{33} \\ 0 & h_{15} & 0 \\ h_{15} & 0 & 0 \\ 0 & 0 & 0 \end{bmatrix} \begin{bmatrix} D_1 \\ D_2 \\ D_3 \end{bmatrix} \quad (2.11)$$

Where $c_{66}^D = \frac{1}{2}(c_{11}^D - c_{12}^D)$.

$$D = dT + \varepsilon^T E \quad (2.12a)$$

$$S = s^E T + dE \quad (2.12b)$$

$$E = -gT + D\varepsilon^T \quad (2.13a)$$

$$S = s^D T + gD \quad (2.13b)$$

$$D = eS + \varepsilon^S E \quad (2.14a)$$

$$S = c^E S + eE \quad (2.14b)$$

$$E = -hS + D/\varepsilon^S \quad (2.15a)$$

$$T = c^D S - hD \quad (2.15b)$$

Equations 2.12 to 2.15 can be used to derive the relations in Table 2.2, which in turn can be very convenient during the analysis of a piezoelectric material

$$\begin{array}{ll}
h = e/\varepsilon^S & c^D = c^E + e^2/\varepsilon^S \\
e = h\varepsilon^S & c^E = c^D - h^2\varepsilon^S \\
d = e/c^E & s^D = 1/c^D \\
g = h/c^D & s^E = 1/c^E \\
\varepsilon^T = \varepsilon^S + e^2/c^E = \varepsilon^S(1 + h^2\varepsilon^S/c^E) &
\end{array}$$

Table 2.2: The relation between the piezoelectric constants.[2]

2.3 Real and imaginary material constants of piezoelectric resonators

The method described by S. Sherrit in [14] determines the complex parameters used in this equation, by considering some critical complex frequencies where the first parallel and serial is given in Eq. 2.16 and Eq. 2.17

$$\hat{f}_p^1 = f_p^1 \left[1 - \iota \frac{f_{-1/2}^{1p} - f_{+1/2}^{1p}}{f_p^1} \right]^{-1/2} \quad (2.16)$$

$$\hat{f}_s^1 = f_s^1 \left[1 - \iota \frac{f_{-1/2}^1 - f_{+1/2}^1}{f_s^1} \right]^{-1/2} \quad (2.17)$$

These frequencies are determined by extracting the given parameters according to Figure 2.5. Considering the admittance as $Y = G + \iota B$ and the impedance as $Z = R + \iota X$, the left plot shows the admittance divided by ω and the right plot the impedance times ω . The critical frequencies are typically maxima and minima in the given figure.

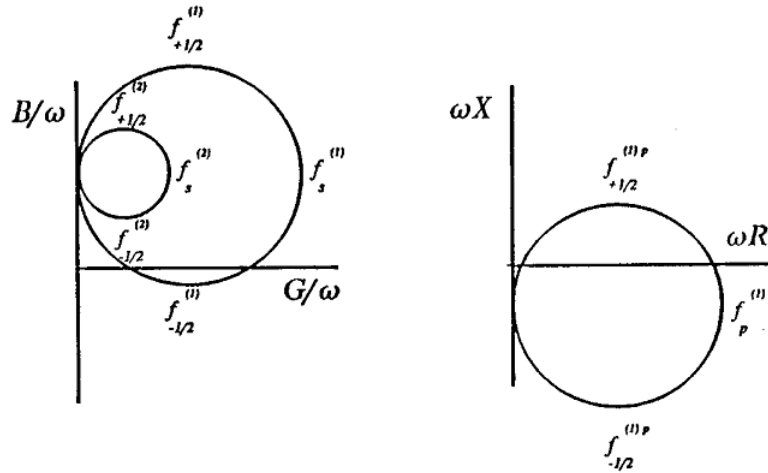


Figure 2.5: Determination of the critical frequencies by admittance and impedance plot [14]

When the \hat{f}_p^1 and \hat{f}_s^1 is found, they contribute to a set of equations describing the material constants given as:

$$k_t^2 = \frac{\pi}{2} \tan \frac{\pi}{2} \frac{f_p^1 - f_s^1}{f_p^1} \quad (2.18)$$

$$c_{33}^D = 4\rho(f_p^1)^2 t^2 / n^2 \quad (2.19)$$

This can also be expressed by

$$c_{33}^D = Zc \left(1 - \frac{1}{Q}\right) \quad (2.20)$$

2.3.1 Loss

All materials are exposed to some kind of loss. Piezoelectric materials have three types of loss, namely dielectric, piezoelectric and mechanical loss. The way we can deal with loss mathematically is to introduce complex parameters. A wave with loss can be described as:

$$e^{-i\frac{\omega}{c}(1-i\alpha)z} = e^{-\frac{\omega}{c}\alpha z} * e^{-i\frac{\omega}{c}z} \quad (2.21)$$

where the wave number k is $\frac{\omega}{c}$. Considering the first factor, we see that this is a decreasing exponential function, dependent of α , which models the wave loss.

The complex permittivity is given as:

$$\epsilon_c = \epsilon' - j\epsilon'' \quad (2.22)$$

where the loss tangent follows the relation $\tan \delta = \frac{\epsilon''}{\epsilon'}$, and is a way to represent the power loss in the medium.

The complex piezoelectric coefficient is given by $h_c = h' - jh''$. The complex stiffness coefficient is given by:

$$c^* = c' - jc'' = c'(1 - j \cdot \tan \delta_m) = c' \left(1 - \frac{j}{Q_m}\right) \quad (2.23)$$

In Equation 2.23 the mechanical loss tangent is given by $\tan \delta_m$ and the inverse of the mechanical Q-factor, Q_m .

Another relation for Q_m given in [14] is

$$Q_m = \frac{\Re\{c_{33}^D\}}{\Im\{c_{33}^D\}} \quad (2.24)$$

A more briefly description of the loss mechanisms in piezoelectric materials is given in [19].

The reason for this is related to the nature of a lossy wave, which can be expressed as:

$$e^{-j\frac{\omega}{c}(1-j\alpha)z} \quad (2.25)$$

$$c_c = \frac{\epsilon''}{\epsilon'} = \tan \delta \quad (2.26)$$

All materials are in some way lossy, this includes piezoelectric materials where three different types of losses occur, namely dielectric, mechanical and piezoelectric loss[26]. These can all be included into calculations through the use of complex permittivity, stiffness matrix and piezoelectric coefficient, respectively.

2.4 Optimization

Through this thesis a Matlab script has been developed in order to search for the correct material parameters. This section will explain some of the mathematical background to give some insight into to process taking place in the script.

2.4.1 Introduction Optimization

Mathematical optimization is a way to find the best element of some set of available alternatives. The selection is based on a criteria, called an objective function $f(\mathbf{x})$, and the goal is to either maximize or minimize this function. The vector \mathbf{x} is an n-vector variable, $\mathbf{x} = [x_1, x_2, \dots, x_n] \in \mathbb{R}^n$, called control variable or decision variable, and the task is to decide \mathbf{x} in order to minimize the objective function. According to[6] this can mathematically be expressed as:

Given a objective function $f : \mathbb{R}^n \rightarrow \mathbb{R}$ which we require to be real valued

$$\mathbf{minimize} \ f(\mathbf{x}) \quad (2.27)$$

If we require that $\mathbf{x} \in \Omega$ we have constraint optimization, otherwise if \mathbf{x} can have all possible vales, we have unconstrained optimization. We also distinguish between two different type of minimizes, namely local and global. As the names suggest they represent a set of decision variables that give the objective function a local or global minima. Through the years many different algorithms has been developed to solve different kind of optimization problems. In this work an algorithm called Nelder-Mead has been applied. A more complete introduction to the field of optimization can be found in either [6] or [9, Chapter 20].

2.4.2 Nelder-Mead Algorithm and fminsearch

The algorithm applied for the optimization script is the Nelder-Mead simplex algorithm. In MATLAB a derived version by Lagarias[10] is implemented in the `FMINSEARCH` function, which is used in this thesis. This algorithm does not use gradients, and is a derivative free method. The mode of operation is by forming a simplex with n+1 points in a n dimensional

search space (in \mathbb{R} the simplex is a line segment, in \mathbb{R}^2 a triangle and so on). By keep track of the function values at the simplex points, the goal is for every iteration to eliminate the point with the highest function value, and swap this with some other with a lower function value. This change can only be done through some specific number of legal moves, which are reflection, expansion, contraction and reduction. These moves are repeated until the diameter of the simplex is beyond the specified tolerance for the answer. For more information about this algorithm, see book [8, Chapter 9]

According to the FMINSEARCH documentation[11], there are some limitations regarding the use of the function. Among them is that the output may not be a global solution, which makes the decision about initial value very important for the outcome. Another limitation is that the function only optimize on real numbers. A work around when dealing with complex decision variables is to split the variable into real and imaginary parts. The function also needs an initial value, which MathWorks recommend to put in close distance to the wanted outcome.

2.5 Uncertainty measurements

To represent the results some statistical tolls has been used. These are found in [7].

Mean Value:

$$\bar{x} = \frac{x_1 + x_2 + x_3 + \dots + x_n}{n} = \frac{1}{n} \sum_{i=1}^n x_i \quad (2.28)$$

Variance:

$$Var(x) = s^2 = \frac{(x_1 - \bar{x})^2 + (x_2 - \bar{x})^2 + (x_3 - \bar{x})^2 + \dots + (x_n - \bar{x})^2}{n - 1} = \frac{1}{n - 1} \sum_{i=1}^n (x_i - \bar{x})^2 \quad (2.29)$$

Standard deviation:

$$s = \sqrt{\frac{\sum_{i=1}^n (x_i - \bar{x})^2}{n - 1}} \quad (2.30)$$

To find the standard deviation for the expression A consisting of multiple measured values, see the following table:

A	Standard Deviation
$A = ax + by + cz$	$s_A = \sqrt{a^2 s_x^2 + b^2 s_y^2 + c^2 s_z^2}$
$A = k * x * y * z$	$s_A = k \sqrt{(yz)^2 s_x^2 + (xz)^2 s_y^2 + (xy)^2 s_z^2}$
$A = k \frac{x}{y}$	$s_A = \frac{k}{y} \sqrt{s_x^2 + (\frac{x}{y})^2 s_y^2}$

Chapter 3

Estimation methods and equipment

In the process of evaluating the complex material constants, mainly two different methods has been applied, but they both based their outcome from the measured electrical impedance. To evaluate the thickness material constant a software optimization script was developed, together with a procedure for choosing the initial value to the script. This is described in Section 3.4. The approach regarding the radial mode parameters derives from a paper by S.Sherrit and is described in Section 3.5.

3.1 Impedance Measurements

Data collection was performed with an impedance analyzer type Agilent 4294A Precision Impedance Analyzer[1]. Due to an upper limit of just 801 sample points, care had to be taken to obtain the necessary data to decide the bandwidth of the signal. Every measurement concerning the piezoelectric disk only, there was performed both a bandwidth of 5MHz and 15MHz, which correspond to a resolution of respectively 6.24 kHz and 18.72 kHz. For the rest of the measurements a bandwidth of 15MHz was applied. The sample was prepared before measurement, by soldering a small copper wire to one of its electrodes. Thereafter the samples were put into a test jig consisting of a copper plate with a clamp that ensured good connection to the copper. The wire from the electrode was connected to the cable from the impedance analyzer through a coax cable with BNZ connector. The purpose of employing this test setup was to ensure better repeatability for each measurement. Experiments also revealed that this setup had some noise reducing effect.

3.2 Fabrication process at ISB

The samples were prepared at the transducer lab at the department. Height measurements were performed with a high precision ($\approx 1\mu$). Measurements were both performed on each layer before adding it to the transducer, and to the whole transducer after the assembly process, to try to gather information from the gluing thickness. Very often the thickness of matching layer 1 had to be justified. This was done by grinding the layer with a specialized

grinding machine. The gluing process was done by a custom build force, which applied a certain force to the transducer during hardening. A temperature chamber to perform baking was also employed.

3.3 xTrans

xTrans is a MATLAB program that makes use of the Mason model to create one-dimensional simulations of piezoelectric transducers. In this thesis it has been used to calculate the electrical impedance, in order to evaluate the object function in the optimization script, where the optimization script connects to the input of xTrans and act like a interface. xTrans has been developed at Department of circulation and medical imaging at NTNU.

3.4 Simulation method for finding the complex thickness parameters

In the process of estimating the complex thickness material constants, an optimization script was written in MATLAB, to function as an interface to xTrans. The idea was to let an optimization algorithm suggest possible values for the material constants, which could be tested out by plotting the electrical impedance in xTrans and then compare this to the measured one. The script make use of the Nelder-Mead optimization algorithm implemented in the FMINSEARCH function in MATLAB. The implementation of the script is given in Section 3.4.1, and the initial setting for the calculation which showed up to be quite affecting to the results is given in Section 3.4.2. The script is capable of optimizing every parameter in SXTRANSPARAM at the same time. Figure 3.1 shows the flow of the script. The X_0 is a vector that can contain all material values in the SXTRANSPARAM struct. As input for the calculation, measured impedance data and which parameters to optimize is requisite. The script search for parameters to try to minimize the objective function ERR, which is given as:

$$err = \sum |\omega Z_{xTrans} - \omega Z_{measured}|^2 \quad (3.1)$$

where $\omega = 2\pi f$ and $Z \in \mathbb{C}$

3.4.1 Implementation of the software

Due to the advanced behavior of complex parameters the development showed up to be quite challenging. To reduce coding time, an already existing MATLAB interface found at MATWORKS website [4] was used as a foundation.

In MATLAB the implementation takes of the objective function takes the form:

```

1 % This is my object code
2 err = sum((2*pi*f(g_ind).')).^2.*((real( Zxd(g_ind) - Zm_aa.Zi.')).^2 + ...
    (imag( Zxd(g_ind) - Zm_aa.Zi.')).^2));

```

The option for for FMINSEARCH was set to:

```
1 initP.options = optimset('MaxFunEvals',1000,'MaxIter',1000,...
2   'Display','final','TolFun', 1e-6,'TolX',1e-6,...
3   'FinDiffType','central','FunValCheck','on');
```

This have impact on the execution of the function, and tell the script to stop searching when the solution has a deviation of 10^{-6} .

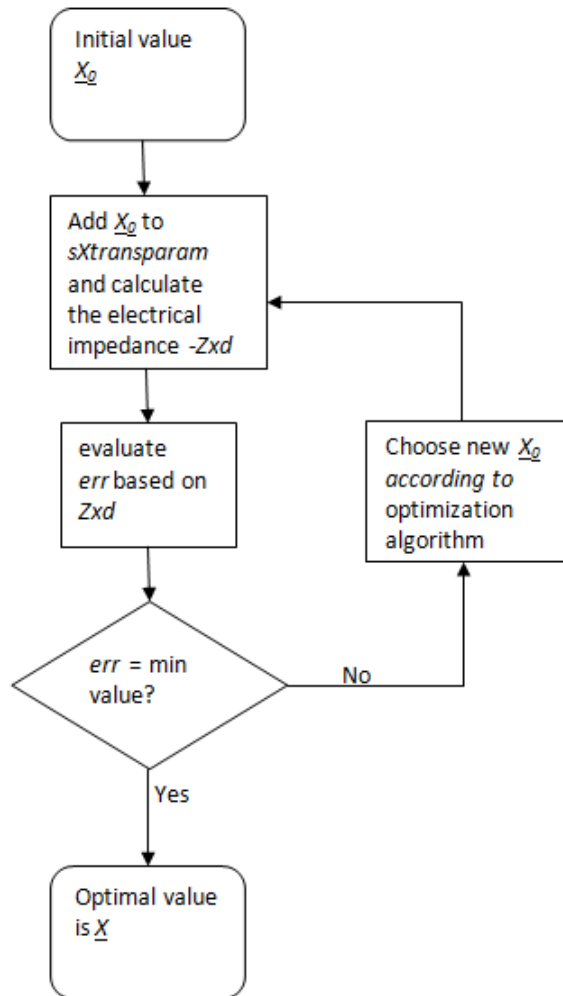


Figure 3.1: Simulation flow

3.4.2 Simulation procedure

The overall philosophy for the simulation is a bottom up approach, assuming each layer is independent. The total amount of layers to simulate is then: pzt disk, Matching Layer

1+glue+air and Matching Layer 2+glue+air. Often the matching layers were regrinded for correct thickness and multiple simulations were done.

From user experience the software script showed up to be quite sensitive for the start up condition. The number of running parameters, the initial value and the sequence did affect the result. One of the reasons to this is that the script stops running if it ends up in a local minimum, although there might be another set of parameters that give a better solution. To deal with this problem, some start up procedure was made.

Firstly the piezoelectric sample is simulated. By measurement, the thickness of the pzt disk with electrodes and the thickness resonance frequency were known. Applying these values into Eq 2.3 reveal the velocity c . The impedance would then be revealed according to Eq 2.1. Hence a set of six parameters is then reduced to four. According to the manufacturer, see Appendix ??, the Q value were given together with a tolerance for the real material constants. As a first guess this Q value was used. As a first guess for the remaining parameters h and ε^S , the values given by the manufacturer including a imaginary part, given in Table 3.1 was used. To find the remaining h and ε , the objective function was replaced with Eq 3.2, so the k_t^2 were optimized. The method given in [14] which were used in my project, gave results concerning k_t^2 and c_{33}^D . For the k_t^2 optimization, the bandwidth which decided which frequencies for the optimizer to run through, was shrinked to just extend the frequencies around the first thickness resonance. The reason for this is that in the calculation of the electrical impedance, the k_t^2 has huge effect of the shape of the resonance peak. The outcome of this simulation gave an estimate for k_t^2 , but also a rough estimate for the relative difference between h and ε^S . This information was used to set the initial values for the simulation using the original objective function. When the k_t^2 simulation was complete, the optimization using the original objective function was used to simulate, h, ε^S and Q. To verify the solution, z, c was also simulated to verify the correct values.

$$err = \frac{h^2 \varepsilon^S}{c_{33}^D} - k_{t-measured}^2 \quad (3.2)$$

where $h, \varepsilon^S, c_{33}^D, k_{t-measured}^2 \in \mathbb{C}$

When it comes to simulation of the rest of the layers, another approach was needed. The layers were glued together, which creates a gap of glue and air bubbles between each layer. This layer has some impact due to the large difference in impedance between air, glue and pzt. When trying to estimate the glue layer with the simulation, the material values for the glue resulted in large deviations from the datasheet. It was then decided to do a SEM inspection in order to get some reliable data about the thickness. The SEM picture, which the initial values for the glue thickness is decided, is given in Appendix B. When simulating the matching layers and the glue layers, material constants for the glue are held constants, according to the datasheet. Therefore only the glue layer thickness and parameters from the matching layer was simulated.

Material Constants	Initial value
ϵ_{33}^S	$914 - j10$
h_{33}	$19.8 + j0.1$
Q	80
<i>Bandwith</i>	normally around 3-5MHz
Glue Layer 1	$10\mu m$
Glue Layer 2	$5\mu m$

Table 3.1: The input value for the start up procedure

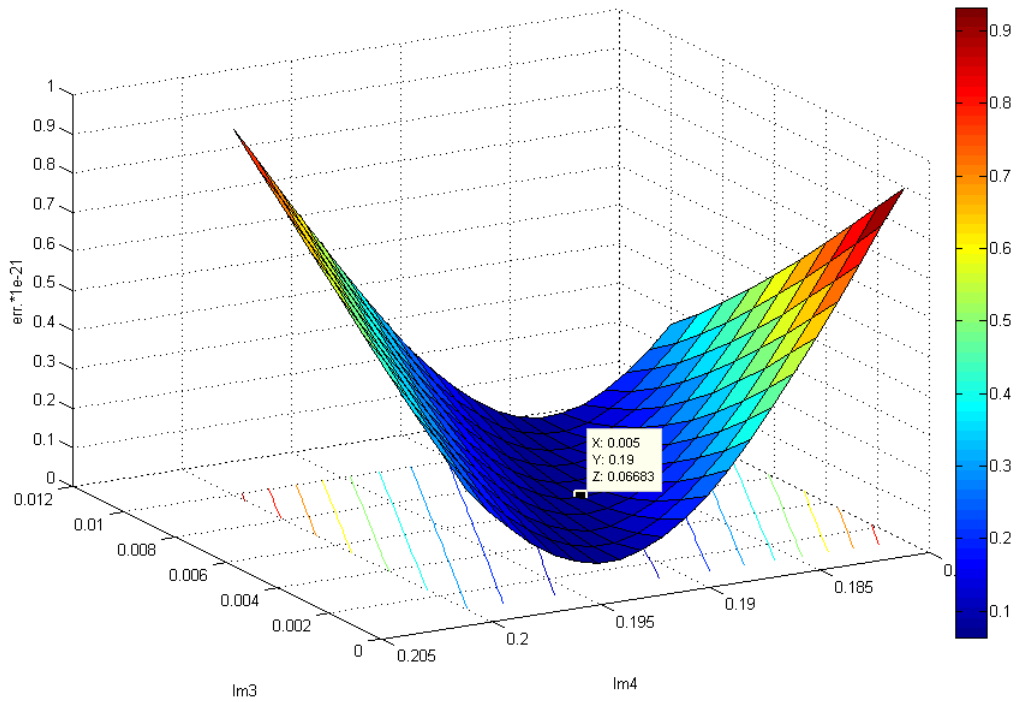


Figure 3.2: Illustrating some of the challenges. $lm3VS_{lm4}$

3.5 Method derived by Sherrit for deriving the radial complex parameters

The method used to evaluate the radial material constants follows the paper of S.Sherrit [15], with some modifications. The paper was published in 1992, and many of the calculations in the paper is based on simplifications to ease, or avoid the use of a computer. This has not been done in this thesis, where the equations are put straight into a MATLAB script. There is also another modification, concerning the extraction of the critical frequencies. Based on my project[18], I found an alternative method which were more robust against oscillations from other resonator modes.

Due to the unevenness of the measured data set, the plot ideally given as Figure 2.5 showed a bad circular behavior, and had great impact on the critical frequencies, which caused large errors on the calculated constants. This was due to the fact that the measurements were done with a limited amount of sample points. To deal with this problem, the extraction of the critical frequencies was performed separately on the real and imaginary graphs. To specifically deal with the limited amount of sample points, interpolation was performed in order to smooth the curves.

In the paper, there was assumed that the ε^T was measured. In our case we only have electrical impedance measurements, so therefore the ε^T was estimated by this data. By assuming for low frequencies that the impedance was pure capacitive, the data could be modeled as Eq 3.3. By assuming that the transducer was acting as a capacitor, following Eq 2.5, the dielectric constant can be found by combine the equations to become:

$$Z = \frac{1}{j\omega C} \quad (3.3)$$

$$\varepsilon^T = \frac{jt}{\omega AZ} \quad (3.4)$$

Important equations used for the calculation is given in Section 2.3. The resulting complex material constants is given in Table 4.8 To verify the accuracy of the developed script, measured data from the paper was used to calculate the material parameters, and compared to the ones published in the paper. The method of obtaining ε^T , is also verified. This verification is given in Appendix A

Chapter 4

Results

In this chapter the resulting thickness parameters made from the optimization script and calculation of the radial parameters are presented. A comparison to reliable sources, for instance the datasheet has been done. Due to lack of data related to the imaginary part, this has been graphically represented and compared to the measured data. Concerning thickness mode parameters, this chapter give the material constants for the piezoelectric disk, the matching layers, and some estimate of the air/glue gap between them. In addition the stiffness constant has been calculated based on the simulated data, calculated based on the method derived in [14]. These have then been compared to the data available from the manufacturer. All results in this thesis is based on the same set of measurements. There have been piezoelectric disks, from the manufacturer Ferroperm-Pizo, with the factory number PZT 27.

4.1 Estimates of the complex material constants for thickness mode

The resulting thickness mode material constants is presented i Table 4.1. The result is the mean value of simulation of a total of four samples. For more statistics related to the results, se Table 4.3,4.4,4.5. When studying the results, it is also advisably to pay attention to Table 4.2, which give the tolerances from the manufacturer on certain constants.

4.1.1 Graphical representation of the admittance

On Fig 4.1 and 4.1 a comparison of the electrical admittance from the simulation(green, red) together with the measured data is presented(blue). The green is the simulated ones, and the red is initial values for this optimization run.

4.1.2 Sources of error

The optimization script accuracy was verified by doing an optimization on a data set from xTrans. The same settings as the real simulation were applied. The optimization succeeded

Variable	Simulated	Datasheet	Deviation %
h (E+8)	19,861675	19,8367	0,13
eps	859,8075	913,73	5,90
Z	34,14	33,347751048609	2,38
c	4434,4415	4330,87675955961	2,39
q	107,37195	80	34,21
Matching Layer 1			
zm2	11,1375	10,3	8,13
cm2	2774,275	2455	13,01
qm2	23,696125	60	60,51
Matching Layer 2			
zm4	2,613625	2,4	8,90
cm4	2159,3	2250	4,03
qm4	22,081825	35	36,91

Table 4.1: Comparison of the real simulated parameters vs. datasheet

Variable	Tolerance	Min value	Max Value %
h (E+8)	$\pm 5\%$	18.81	20.79
eps	$\pm 10\%$	822.6	1005.4
q	$\pm 2.5\%$	78	82

Table 4.2: The tolerances from the manufacturer

Variable	Mean		Variance		Standard Deviation	
	Real	Imag	Real	Imag	Real	Imag
h	19,8617	0,0980	0,8228	0,0001	0,9071	0,0072
eps	859,8075	-9,7584	4514,3907	0,9560	67,1892	0,9778
Z	34,1400	34,1400	0,0061		0,0783	
c	4434,4415		96,6767		9,8324	
q	107,3720		371,3327		19,2700	
l	0,5118		0,0000		0,0030	

Table 4.3: A statistical representation of the material constants for the piezoelectric disk

Variable	Mean		Variance		Standard Deviation	
	Real	Imag	Real	Imag	Real	Imag
Matching Layer 1						
zm2	11,1375		0,5095		0,7138	
cm2	2774,2750		2238,8092		47,3161	
qm2	23,6961		63,1859		7,9490	
lm2	0,1390		0,0001		0,0073	

Table 4.4: A statistical representation of the material constants for the Matching Layer 1

Variable	Mean		Variance		Standard Deviation	
	Real	Imag	Real	Imag	Real	Imag
Matching Layer 2						
zm4	2,6136		0,0449		0,2118	
cm4	2159,3000		12955,3533		113,8216	
qm4	22,0818		9,1228		3,0204	
lm4	0,1467		0,0003		0,0178	

Table 4.5: A statistical representation of the material constants for the Matching Layer 2

Variable	Mean	Standard Deviation
Glue Layer 1		
lm1	0,0113	0,0028
Glue Layer 2		
lm3	0,0064	0,0016

Table 4.6: A statistical representation of the thickness of the glue

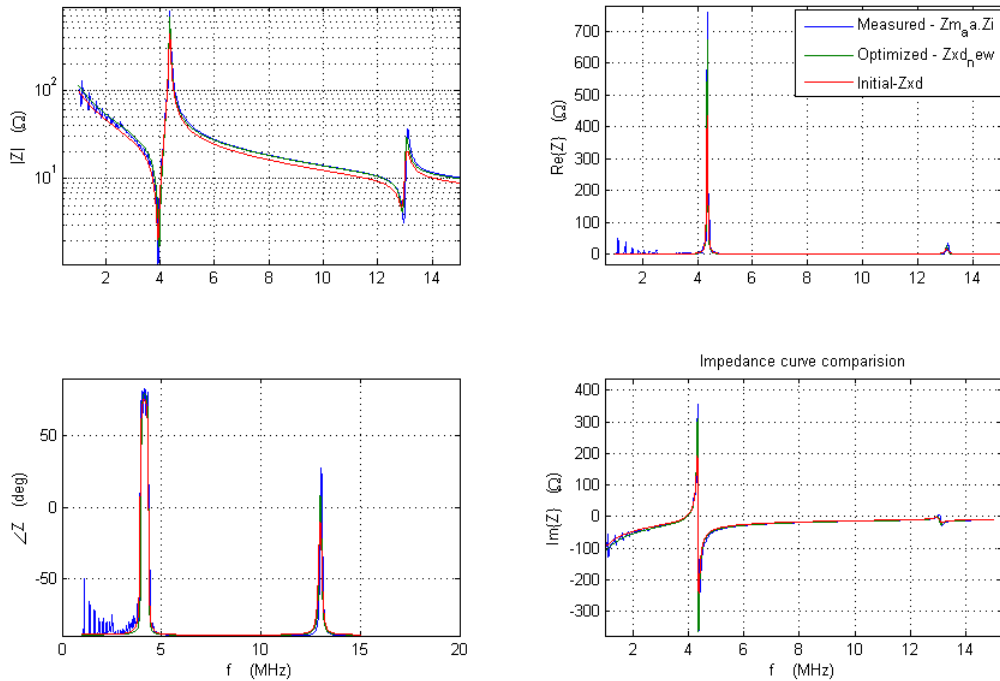


Figure 4.1: Sample 4 Simulated for PZT layer

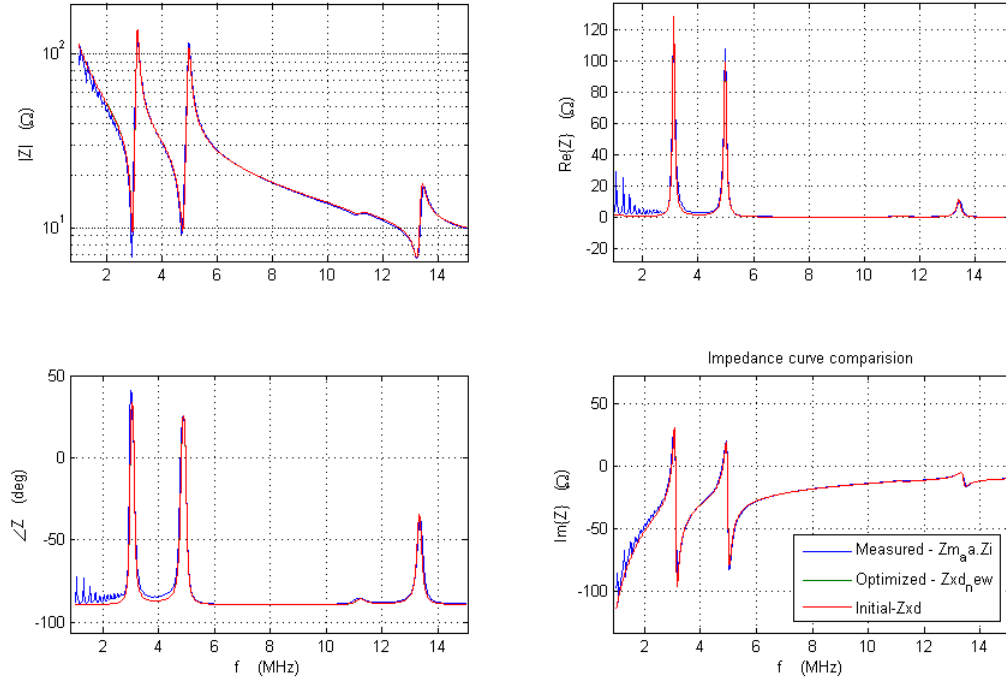


Figure 4.2: Sample 4 Simulated for ML1 layer

with an error of 0!. This means that the script is capable, during perfect initial conditions, to find the global minimum. It must be added that the accuracy tolerance, was in accordance with the rest of the simulation, which is 10^{-6} , so the objective function $ERR \leq 10^{-6}$

4.1.3 Comparison of the modeled admittance curve and the measured

By inserting the simulated material constants into xTrans, the admittance curve was calculated and compared to both measured data, and calculated admittance curve based on datasheet data. The comparison is illustrated in Figure 4.4, which give a motivation for using complex material constants. The red curve shows the xTrans curve based on real parameters from the datasheet, the green shows xTrans data with optimized complex constants, and the blue is the measured data. Figure 4.5 is a zoomed version of the same plot and reveal a slightly better fit using the complex vales. These figures illustrate the absolute vale and the phase of the curve, since comparing the real and imaginary parts does not give information in this setting.

4.1.4 SEM inspection of the samples

Due to the fact that the simulation of the thickness of the glue gave results with large deviation from the datasheet, it was decided to do a physical check. There was one transducer that

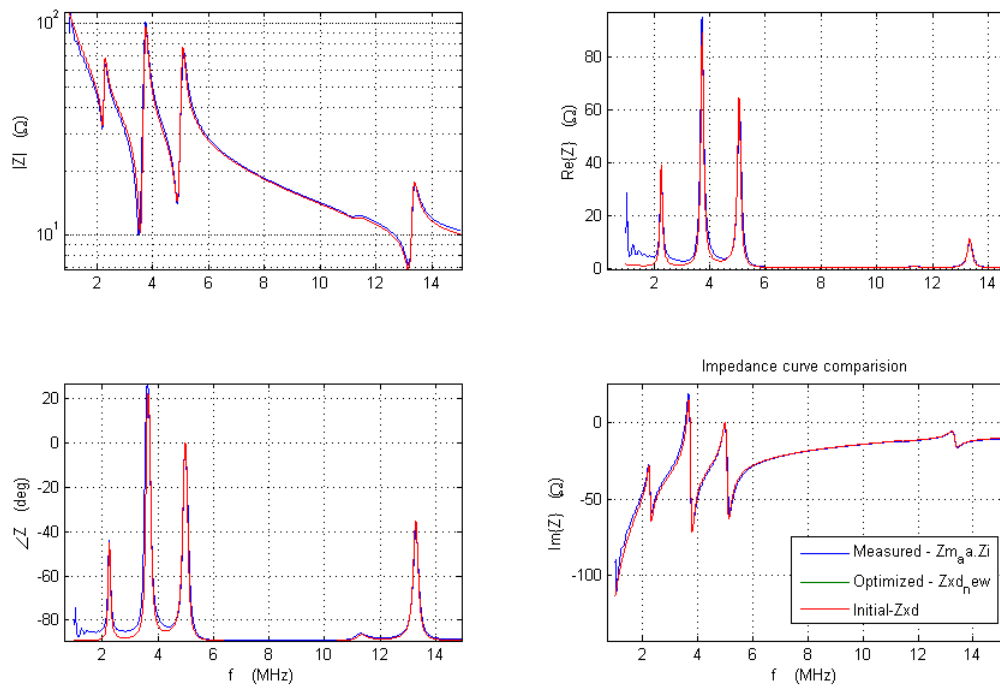


Figure 4.3: Sample 4 Simulated for ML2 layer

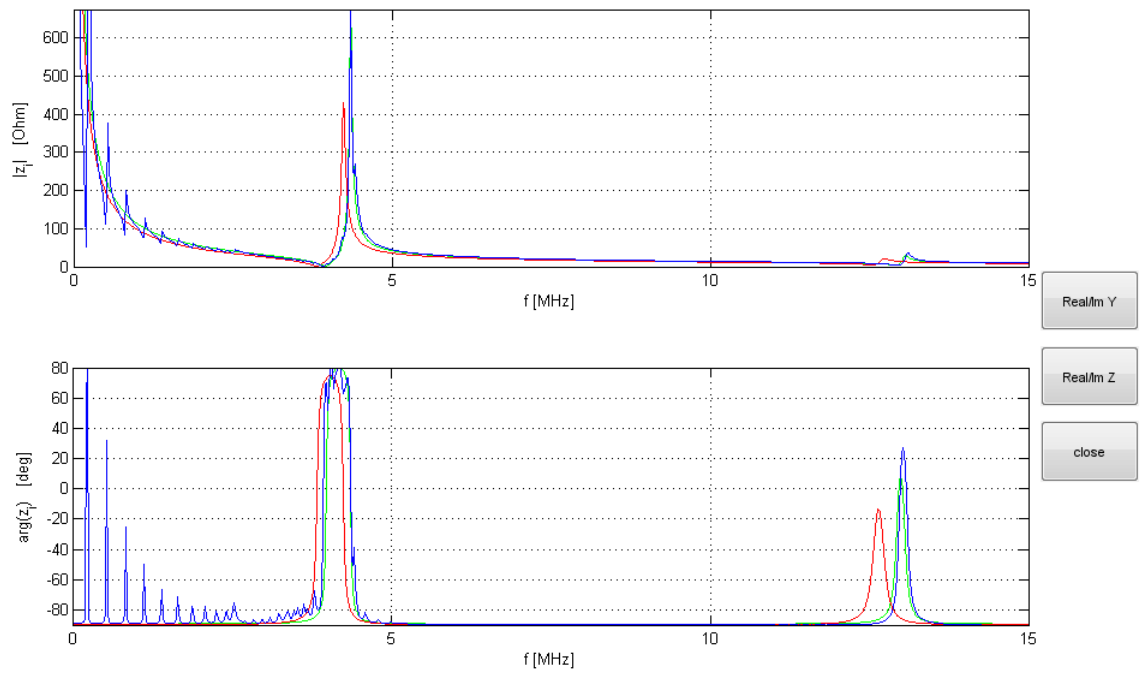


Figure 4.4: Comparison of the complex material constants and the real to the measured data

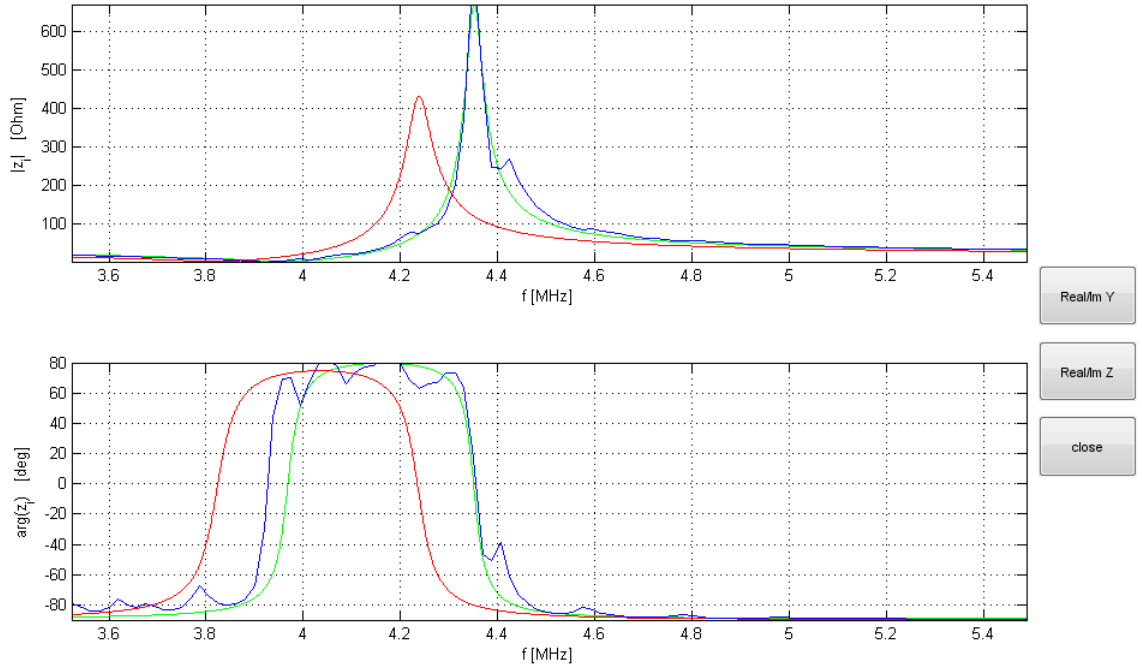


Figure 4.5: Same as above but zooming in on the essential parts

during production showed bad behavior, so this was cut into two pieces so the cross section was revealed. A tabletop Scanning Electron Microscope at the NTNU NanoLab was used to take pictures of the cross section. These pictures are presented in Appendix B. Based on findings from these pictures, the initial values of the glue thickness were decided. Probably this examined sample had too large gaps, so there might be smaller gaps in those that are simulated, due to the bad behavior.

4.1.5 Derived material constants

Based on the simulation a set of material constants was calculated. Among them is the stiffness constant c_{33}^D . The stiffness constant has been calculated by the optimized values, using the Equation 2.20. Table 4.7 shows the calculated values compared to the ones found in the datasheet.

c_{33}^D has also been calculated another way, by the use of the method from [14] which gave the value $1.514575+0.011626i$.

		Calculated C based on simulated values Mean	C based on values from datasheet
PZT	e+11	1.5139-0.014448i	1.444-0.01805i
Lim 1	e+9	6.86-0.52769i	6.86-0.527692i
ML1	e+10	3.0921357-0.144455i	2.52865-0.04214i
Lim 2	e+9	6.86-0.527692307i	6.86-0.527692307i
ML 2	E+9	5.63251-0.257336601i	5.40-0.154285714i

Table 4.7: Comparison of c33d

4.2 Evaluation of the complex material constants in the radial mode

The radial mode material constants is all calculated a developed MATLAB script in accordance with the paper [15]. The accuracy of the script has been verified by calculating the results from the paper. The verification is given in Appendix A. Note in accordance with [15], these material constants is only valid in near distance to the first resonance peak.

A table of the resulting material constants is given in Table 4.8:

Parameter	Ferroperm	Magnitude	Sample 4	Sample 8	Sample 12
s11E	1,69555E-011	E-11	1.4263-3.3624e-2i	1.3740 -1.2521e-2i	1.4332 -2.4562e-2i
s12E	-6,5991E-012	E-12	-5.0937 -3.7083e-1i	-6.9973 -4.8490e-1i	-6.4920 -5.6096e-1i
d31	-1,699915E-010	E-12	-155.21 +8.4805i	-127.60 +7.6445i	-134.08 +7.3514i
epsilonT		E-8	1.5696 -2.3037e-2i	1.5097-1.5490e-2i	1.6312 -2.1468e-2i
c11p		E10	7.0073 +1.6520e-1i	7.2773+6.6313e-2i	6.9752+1.1954e-1i
σ_p	0,3892	-	0.3563 + 0.0344i	0.5089 + 0.0399i	0.4522 + 0.0469i
k^p		-	0.5843 + 0.0023i	0.5954 + 0.0067i	0.5320 + 0.0233i
epsilonP		E-8	1.0444 -6.1164e-3i	1.0272 -1.2796e-3i	1.1737-1.8252e-2i

Table 4.8: The result from samples used.

Uncertainty calculations for the material parameters is given in Table 4.9

On Fig 4.6 and 4.7 shows comparison of the electrical admittance, for the measured date, and the calculated. The green curve shows a interpolation of the measured data(blue), and the red is the one calculated by the admittance equation from the paper.

In Figure 4.7 the real and imaginary parts are revealed.

Parameter	Mean		Varians		Standard avvik	
	Real	Imag	Real	Imag	Real	Imaginr
s11E	1,4112	-0,0236	0,0010	0,0001	0,0324	0,0106
s12E	-6,1943	-0,4722	0,9724	0,0092	0,9861	0,0957
d31	-138,9633	7,8255	208,4632	0,3433	14,4383	0,5859
epsilonT	1,5702	-0,0200	0,0037	0,0000	0,0608	0,0040
c11p	7,0866	0,1170	0,0275	0,0024	0,1659	0,0495
σ_p	0,4391	0,0404	0,0059	0,0000	0,0771	0,0063
k^P	0,5706	0,0108	0,0011	0,0001	0,0339	0,0111
epsilonP	1,0818	-0,0085	0,0064	0,0001	0,0801	0,0087

Table 4.9: Uncertainty calculations of the calculated parameters

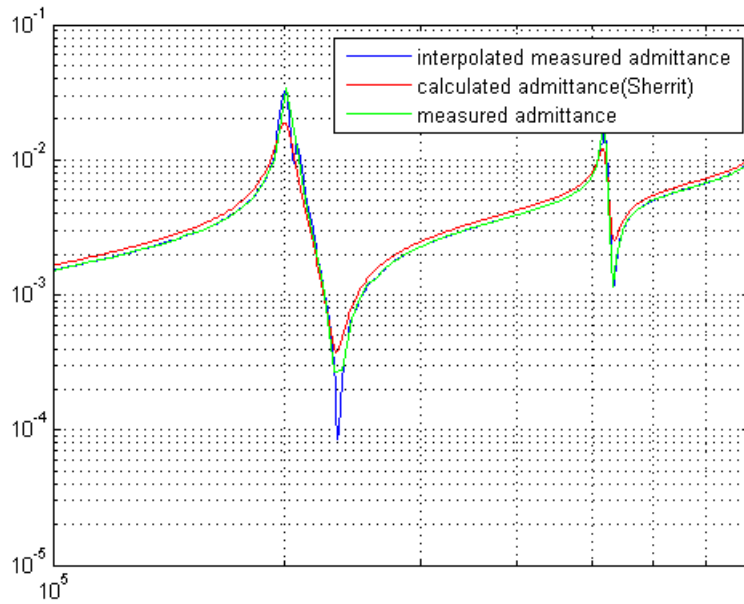


Figure 4.6: loglog plot of sample 4, which shows great fit

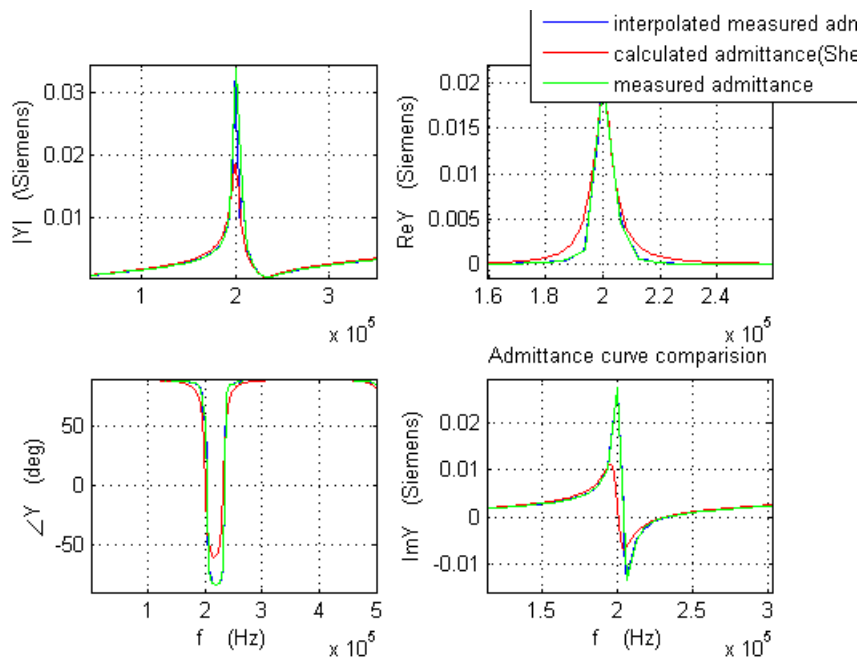


Figure 4.7: Sample 4

Chapter 5

Discussion

The development of the optimization script showed up to become a huge challenge concerning the programming and the development of the mathematical implementation. The fact that this optimization problem was in the complex domain, special consideration related to the optimization function had to be made, for correct input. During this process, other types of optimization were investigated. The options were to whether find some free source code specifically written for complex optimization from the web, or use the existing optimization toolbox in Matlab. Due to the fact that xTrans, which is an important part of the optimization, is written in Matlab, the easiest solution was to use the MATLAB solution. Dealing with the mathematics concerning these algorithm was of the edge of the mathematics curriculum during my time at NTNU, but thanks to great user guides on MATLAB website, I did get it to work. The script which was developed can deal with many free parameters, which makes it ideal when doing simulation on multiple layers. The biggest drawback is that it is very sensible to the initial value, and the solution might be just a local solution. To help with that a initial value procedure was made, which made some improvements. Although for future user this method might be too unstable, that the result will be trusted.

When it comes to evaluation of the outcome of the script, it is hard to verify the accuracy, because there are now known imaginary data available for these transducers. Although the verification of the script showed zero error, the solution is not guaranteed to be a global solution. As a consequence the outcome can be an optimal solution, given the free parameters, but not for the whole sample. To deal with this problem, software which uses global optimization algorithm must be employed. The outcome of this simulation, does give a good picture of the physical process taking place in the transducer, as Figure 4.4 reveal, where we see an improvement of the fitting by the complex material constants compared to the ones from the datasheet. The biggest motivation for introduce complex material constants is to include loss in each particular parameter. When doing simulation on the piezoelectric sample, very often there was a divergence between the piezoelectric constant, dielectric constant to the Q factor. This might have something to do with the introduction of loss.

The method used to calculate the radial material constants was already described by S.Sheritt. The characteristic frequencies used to make the complex frequencies, had to be measured at a very low frequency, where the shape of the curve was bad due to few measurements points. Although interpolation was introduced, this did not give the expected outcome. Evaluation

of the outcome of the radial calculation can be done by studying Table 4.8. We see that some of the constants, do have large deviation, compared to the datasheet values. It should be emphasized that these results derived from this method, is valid in close range to the first resonance peak.

Chapter 6

Conclusion and Further Work

The main goal of this thesis has been to establish a method and estimate the complex material constants for the radial and thickness mode. The motivation to introduce complex material constants is to include loss in each particular material constant, and not only a loss parameter. Very often the manufacturer only publishes its real material constants, which is also the case for the sample used in this simulation. This gives us very little data to verify the estimation. The estimated constants have been compared to the real values given in the datasheet, but we have no proper data that can give indication of the accuracy of the estimation regarding the imaginary parts of the constants. However an evaluation of the constants based on comparison of the admittance of the measured data to the optimized constants has been made. When plotting the absolute value, and its phase, the complex constants show a slightly better fit, than the ones described in the datasheet. Therefore it is likely to consider the complex material constants found in this thesis to give good information about the process in the transducer.

Due to the local/global minima uncertainty, the outcome of this optimization method may vary according to the initial value. For materials where a proper initial value is known, this method can be of certain benefit. Further work in this field, should use other type of algorithm and objective function. This requires a deep understanding in math, and computer science. If a good algorithm is established, the framework made by the source code and the way of connecting to MATLAB can be interesting contributions from this method. One should also try this method to another type of material, which can reveal a better understanding of the initial value problem. If there exist a material with known complex material constants, an evaluation of these, using this method will reveal a bigger understanding regarding the accuracy compared to the initial value

The method published by S.Sherrit has been evaluated, and the material constants calculated showed conformity to the real data, although the uncertainty is high. A more comprehensive investigation regarding the statistical coherence of the complex material constants would also be of interest.

Bibliography

- [1] AGILENT. Operation manual - agilent 4294a precision impedance analyzer, November 2002.
- [2] ANGELSEN, B. A. J. *Ultrasound Imaging Waves, Signals and Signal Processing Vol 1*. Emantec Norway, 2000.
- [3] AULD, B. A. Wave propagation and resonance in piezoelectric materials. *The Journal of the Acoustical Society of America* 70, 6 (1981), 1577–1585.
- [4] BOYNTON, G. fminsearch interface - File Exchange - MATLAB Central, Sept 2005.
- [5] COBBOLD, R. S. *Foundations of biomedical ultrasound*. Oxford University Press, 2006.
- [6] EDWIN K.P. CHONG, S. H. Z. *An Introduction to OPTimization 3th ed*. Wiley, 2008.
- [7] HAMMER, E. *Instrumenter og mleteknikk*. Universitetsforlaget, 1977.
- [8] JORGE NOCEDAL, S. J. W. *Numerical Optimization 2th ed*. Springer, 2000.
- [9] KREYSZIG, E. *Advanced Engineering Mathematics 8th ed*. Wiley, 1999.
- [10] LAGARIAS, J. C., REEDS, J. A., WRIGHT, M. H., AND WRIGHT, P. E. Convergence properties of the NelderMead simplex method in low dimensions. *SIAM Journal of Optimization* 9 (1998), 112–147.
- [11] MATHWORKS. Find minimum of unconstrained multivariable function using derivative-free method - matlab, January 2012.
- [12] NTNU. Smart microsystems for diagnostic imaging in medicine, April 2011.
- [13] PUBLICATIONS, E. Seeing Into the Future: Medical Imaging and Diagnostics Guide Advances in Healthcare, Jan 2011.
- [14] S. SHERRIT, H.D. WIEDERICK, B. M. Pdp 135 non-iterative evaluation of the real and imaginary material constants of piezoelectric resonators. *Ferroelectrics* 134 (1992), 111–119.
- [15] SHERRIT, S. Accurate evaluation of the real and imaginary material constants of piezoelectric resonator in the radial mode. *Ferroelectrics* 119 (1991), 17–32.
- [16] SHUNG, K. *Diagnostic Ultrasound, Imaging and blood Flow Measurments*. Taylor and Francis Group, LLC, 2006.
- [17] STD 176-1987, A. IEEE Standard on Piezoelectricity.

- [18] TJELDE, E. Characterization and parameter estimation of the piezoelectric layer in an ultrasound disk transducer. *Unpublished* (2011).
- [19] UCHINO, K., AND HIROSE, S. Loss mechanisms in piezoelectrics: how to measure different losses separately. *Ultrasonics, Ferroelectrics and Frequency Control, IEEE Transactions on* 48, 1 (Jan. 2001), 307 –321.
- [20] VECTOR. Versatile endoscopic capsule for gastrointestinal tumor recognition and therapy, April 2011.
- [21] WASER, R. *Nanoelectronics and Information Technology, Advanced Electronic Materials and Novel Devices Second edition*. Wiley-VCH, 2005.
- [22] WIKIMEDIA. Perovskite structure of pzt, May 2011.
- [23] YANG, J. *An Introduction to the Theory of Piezoelectricity*. Springer Science, 2005.

Appendix A

Accuracy on the calculation script

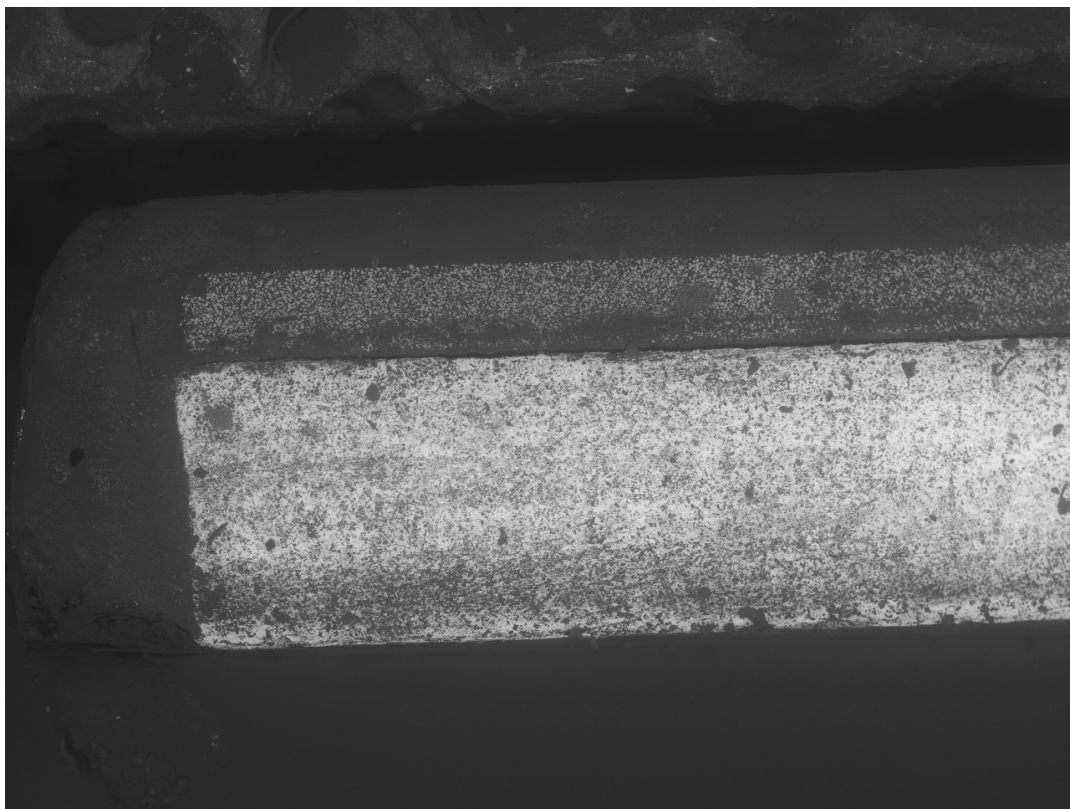
This table shows the accuracy of the developed script

Parameter	Magnitude	Calculated results	Sherrit Values	Error %	
				Real	Imag
s11E	E-11	1.4628(1-0.023611i)	1.704(1-0.01832i)	14,15	10,64
s12E	E-12	-5.4894(1-0.02278i)	-6.394(1-0.02496i)	14,15	21,65
d31	E-12	-205.9(1-0.03057i)	-222.5(1-0.02364i)	7,46	19,67
epsilonT	E-8	2.7337(1-0.02077i)	2.740(1-0.02077i)	0,23	0,23
c11p	E10	6.8343(1+0.01614i)	6.829(1+0.01614i)	0,08	0,08
Poisson Ratio $-\sigma_p$	-	0.3753 - 0.0025i	0.3753(1-0.00664i)	0,00	0,32
k^p	-	0.5946 - 0.0060i	0.5945(1-0.01013i)	0,02	0,37
epsilonP	E-8	1.8062(1-0.0062i)	1.810(1-0.01450i)	0,21	57,33

Table A.1: Comparison of the parametrs given in the paper and the one calculated with the developed radial script

Appendix B

SEM inspection of a transducer sample



2011.11.09 F L D6,2 x120 500 um

Figure B.1: The edge

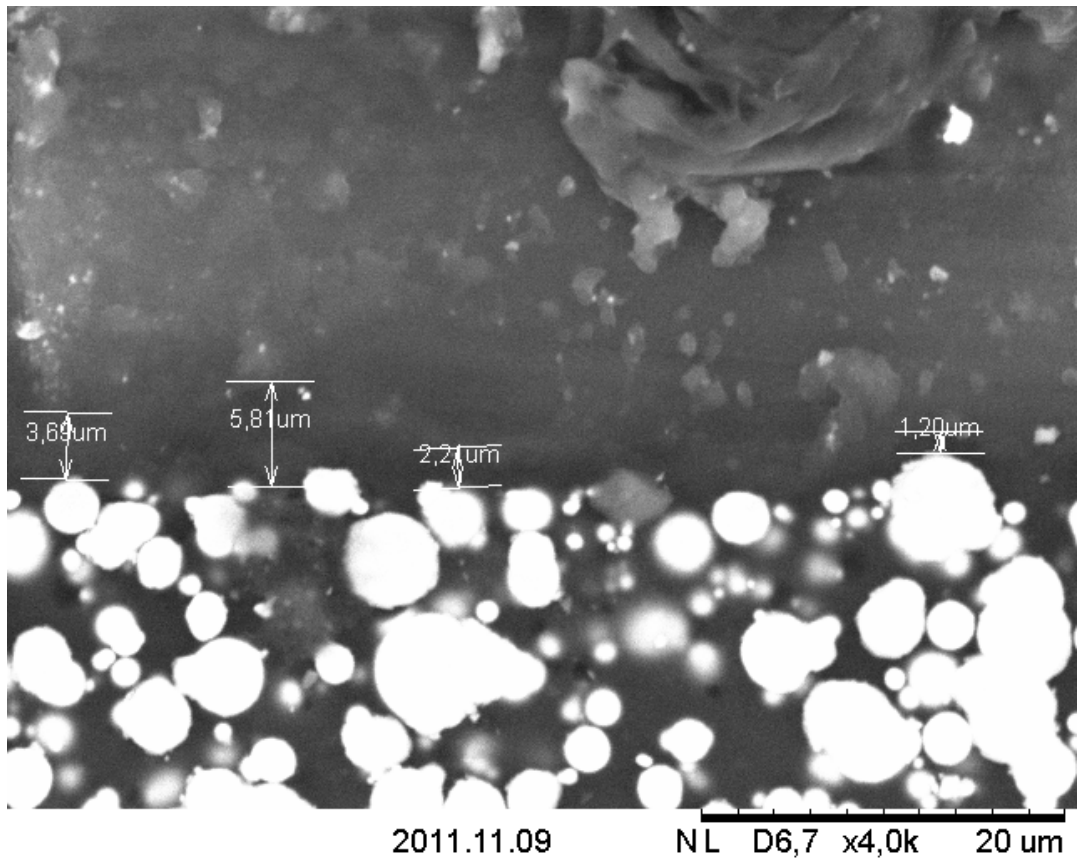


Figure B.2: Showing the consisting of glue and air

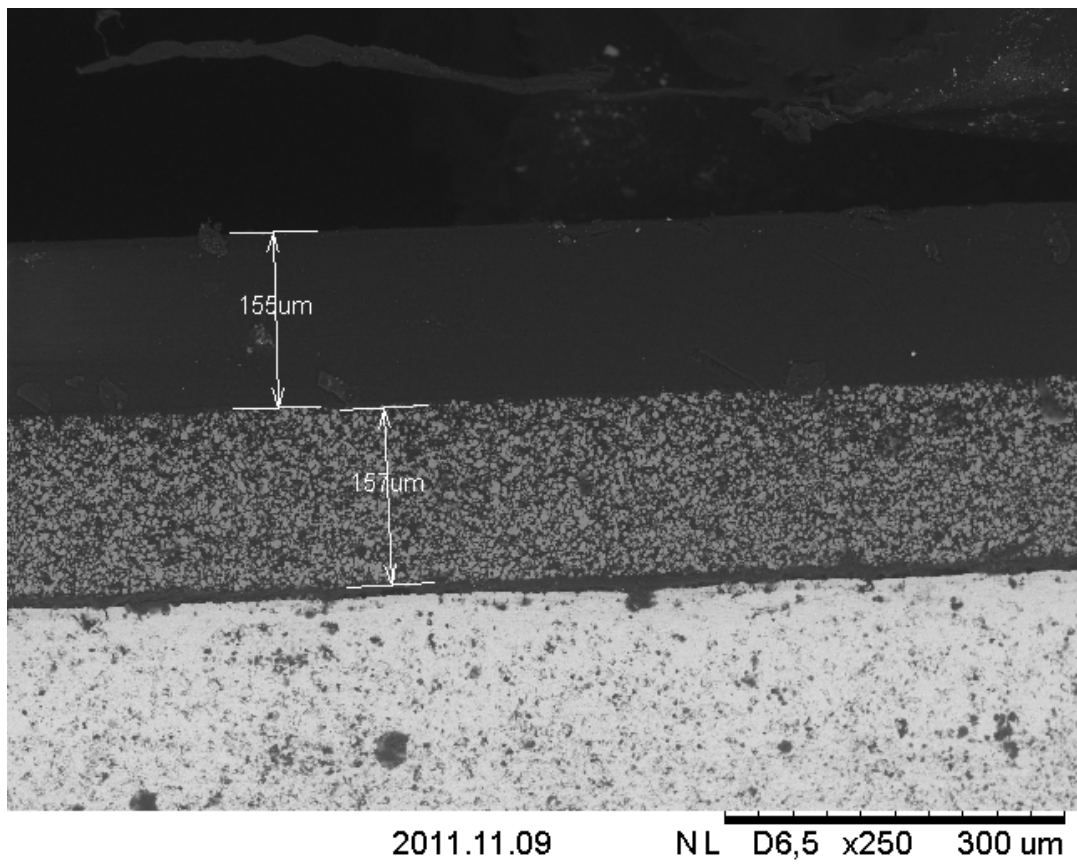


Figure B.3: SEM3

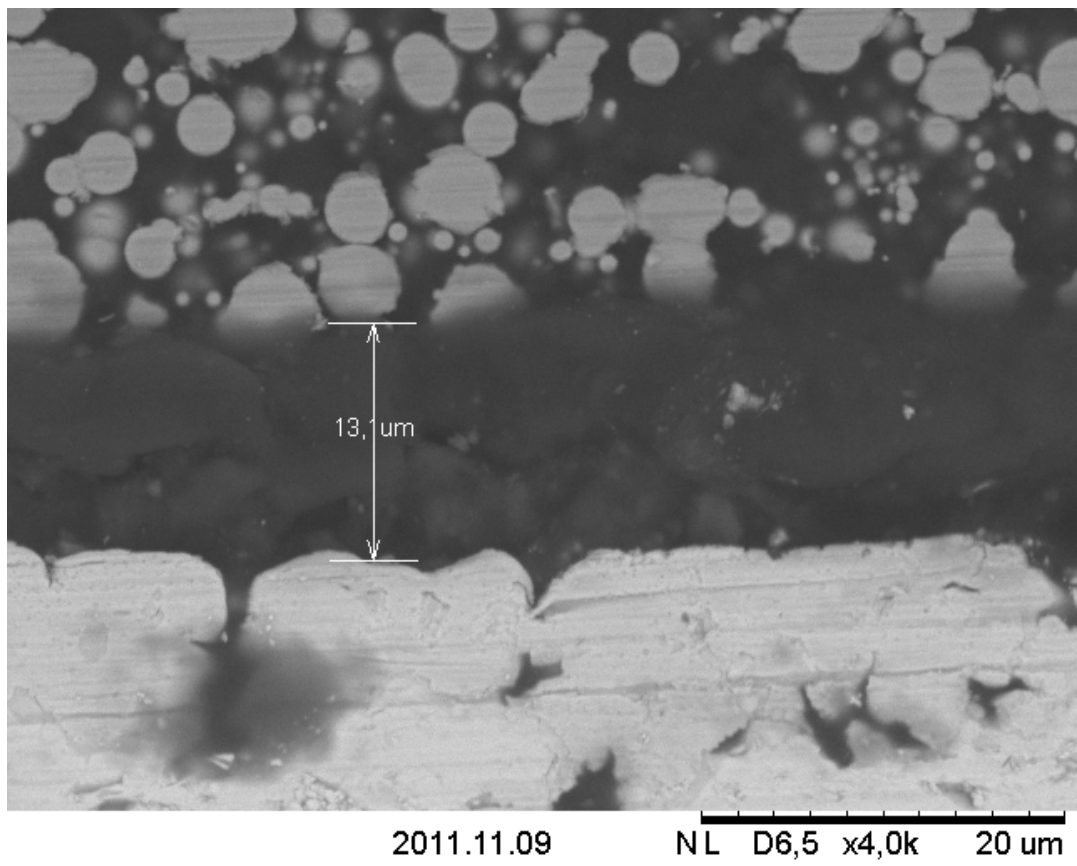


Figure B.4: SEM4

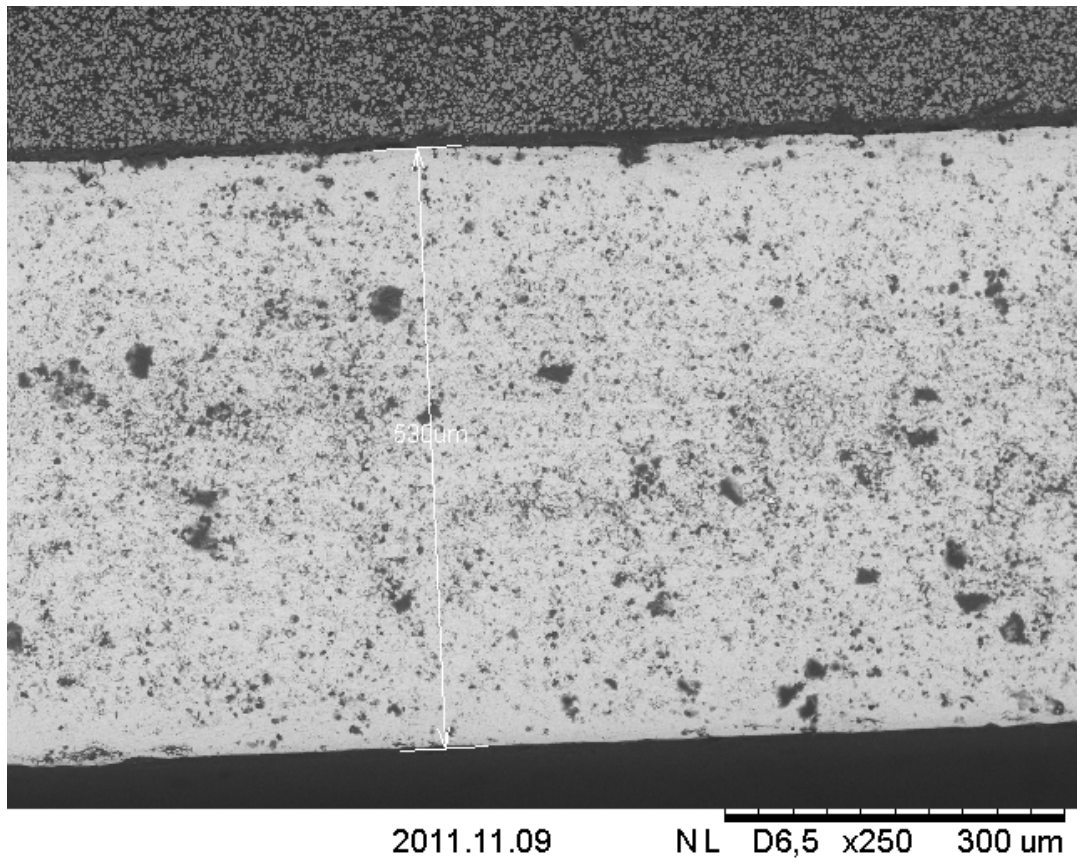
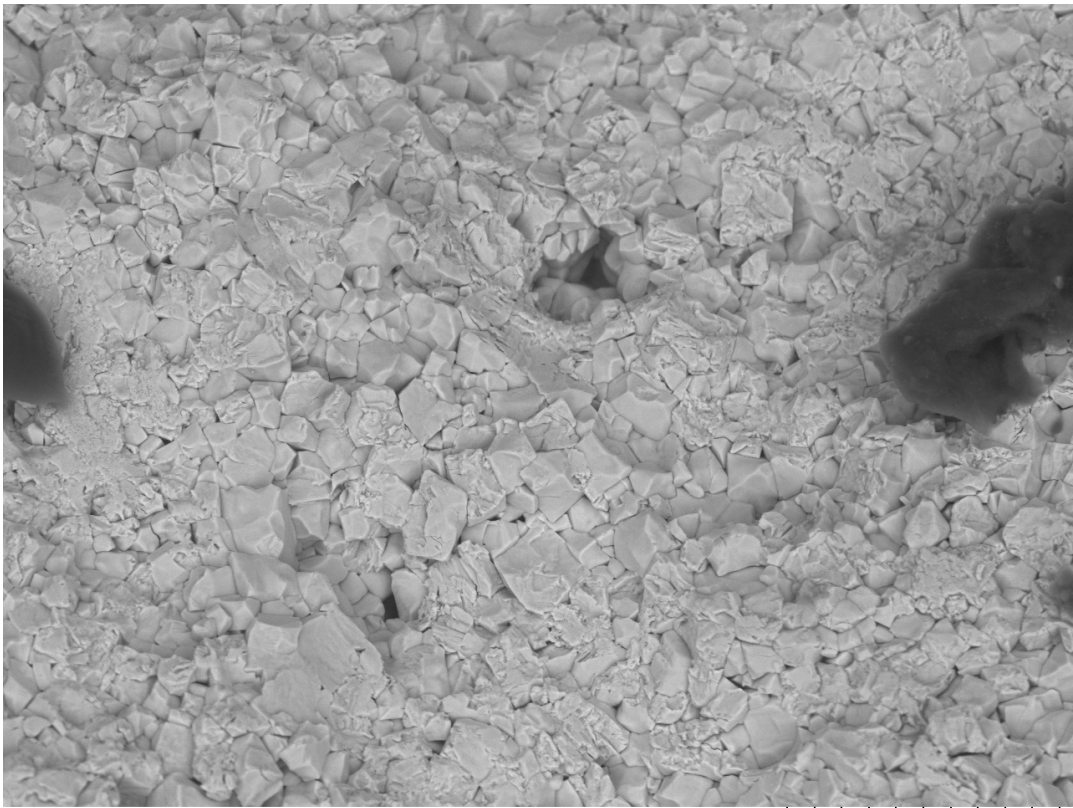


Figure B.5: SEM5



2011.11.09 NL D4,7 x2,0k 30 um

Figure B.6: SEM6



2011.11.09 NL D5,0 x2,0k 30 um

Figure B.7: PZT grain size